Electronic supplementary information

Improving quantum efficiency in organic solar cells with a small energetic driving force

Haiqin Liu, [a] Mengyang Li, [a] Hongbo Wu, [a] Jie Wang, [a] Zaifei Ma, [*a] Zheng Tang [*a]

[a]State Key Laboratory for Modification of Chemical Fibers and Polymer Materials, Center for Advanced Low-dimension Materials, College of Materials Science and Engineering, Donghua University, Shanghai, 201620, P. R. China

Email: ztang@dhu.edu.cn; mazaifei@dhu.edu.cn

Table of Contents

SI-1. Experimental

Characterizations: The thickness of the films in this manuscript were all determined by the profilometer of KLA-Tencor P-7 Stylus Profiler. The J-V characteristics curves of the solar cells were measured under simulated AM 1.5 G illumination (100 mW cm^2) with a solar simulator (Newport Oriel VeraSol-2™ Class AAA), calibrated using a set of low-pass optical filters and a Si photo diode. EQE spectra were measured with a halogen lamp, a monochromator (CS260-RG-3-MC-A, Newport), an optical chopper with a frequency of 173 Hz (3502 Optical Chopper, Newport). The diameter of the illumination spot is reduced to approximately 0.5 mm using a focus lens. A DC bias light (LSH-75, Newport, 250W) is used during the measurement, and the AC current signals from the solar cells were amplified using a current amplifier (Stanford University, SR570), and then collected by a lock-in amplifier (Stanford University, SR830). For the EQE_{EL} measurements, a digital source meter (Keithley 2400) is used to inject electric current into the solar cells, and the emitted photons are collected by a Si diode measured by a picoammeters (Keithley 6482).

Electroluminescence measurements were done using a source meter (Keithley 2400) to inject electric current, and the emitted photons were measured using a fluorescence spectrometer (KYMERA-3281-B2, Andor) with two sets of diffraction gratings, a Si EMCCD camera (DU970P-BVF, Andor) for the wavelength range of 400~1000 nm, and an InGaAs camera (DU491A-1.7, Andor) for the wavelength range of 900~1600 nm. Photoluminescence measurements were done using a laser excitation (460 nm), and the emission spectra were obtained using the same setup used for recording electroluminescence spectra. The transient photovoltage decay measurements were done using two white LED lamps, driven by a Keithley 2450 source meter for different bias illumination intensities and an arbitrary function generator (AFG3022C, Tektronix) for the transient illumination. The peaks of the transient voltage signals, recorded by an oscilloscope (MDO4104C, Tektronix), were kept to approximated 5% of the DC bias photovoltage signal, by adjusting the driving voltage of the LED controlled by the function generator for each bias illumination intensity, and the record transient photovoltage decay signals were fitted using an exponential decay function for determining the decay time constants.

SI-2. Details regarding the determination of CT state energy in organic solar cells

The tails of the EQE spectra are determined by a sensitive EQE setup, which consists a halogen lamp, a monochromator, a current amplifier and a lock-in amplifier. A set of long pass filters are used to make sure that the higher order wavelengths from the monochromator are completely cut off and light reaching the device under test is truly monochromatic. To further extend the range of the EQE spectra measured by the sensitive EQE setup, electroluminescence (EL) spectra of the solar cells are also measured, using a small injection current (1 mA). Because EL spectra of the BHJ organic solar cells are dominated by CT state emission, they can be converted to CT state absorption spectra using the reciprocal relation [*Phys. Rev. B* **2007**, *76*, 085303.].

$$EL(E) = EQE(E)\phi_{BB}(E)[\exp\left(\frac{qV}{kT}\right) - 1]$$

By attaching the CT absorption spectra calculated from EL to the EQE spectra measured with the sensitive EQE setup. We obtain complete EQE spectra spanning over 8 orders of magnitude for all of the solar cells investigated in this work. As an example, the complete EQE and EL spectra for the binary solar cell based on PM7:Y5 are shown in Fig. S1. The tail of the EQE spectrum, corresponding to CT absorption, can be used to determine the energy of CT state (E_{CT}) by a fit using the equation derived in the framework of Marcus theory [*J. Phys. Chem.* **1989**, *93*, 3078.].

$$EQE(E) = \frac{fE}{\sqrt{4\pi\lambda kT}} exp(-\frac{(E_{CT} + \lambda + E)^2}{4\lambda kT})$$

To avoid an arbitrary fitting, two boundary conditions are imposed. First, we calculate the lower limit for the radiative recombination voltage loss ($V_{r,sq}$) for a solar cell as a function of E_{CT} using the Shockley-Quessior theory, assuming that E_{CT} is the effective energy of the bandgap of an organic solar cell. Then, the Gaussian region in the lower energy part of the EQE spectrum of the solar cell based on PM7:Y5 is selected and fitted. During the fitting process, a set of f values typically in the range between 0.0001 to 0.1 are used as constant input values, while E_{CT} and λ are left as fit parameters. As a result, we obtain a range of values for E_{CT}, which are used to calculate ΔV_r, using the simple equation:

$$\Delta V_r = \frac{E_{CT}}{q} - \Delta V_{oc} - \Delta V_{nr}$$

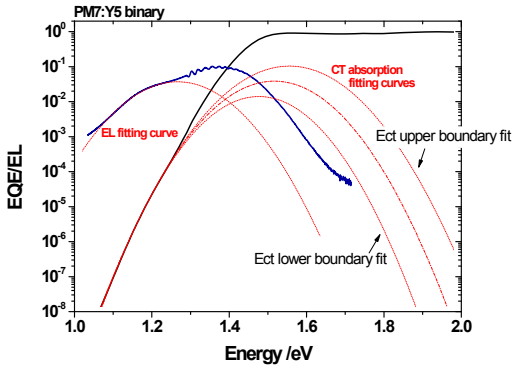

Fig. S1. EQE and EL spectra of the binary solar cell based on PM7:Y5. A series of fittings are performed to find the range of values for E_{CT} with a realistic physical meaning.

The calculated ΔV_r values are compared to $\Delta V_{r,sq}$ from the Shockley-Quessior theory, and the E_{CT} values leading to ΔV_r smaller than $\Delta V_{r,sq}$ are ruled out. By doing so, we determine the minimal value for E_{CT}, which is 1.37 eV for the solar cell based on PM7:Y5. Then, we determine the EQE spectrum solely due to CT absorption, using the Marcus equation and the fit results. A loose upper boundary for E_{CT} is that the EQE of CT state absorption should always be lower than the that of the absorption of the singlet states in the solar cell. Therefore, the E_{CT} values giving rise to CT state EQE higher than the EQE of the singlet states are also ruled out. In fact, the CT state EQE should be much smaller

than the singlet state EQE, due to the considerably weaker CT state absorption strength. To our knowledge, the highest CT state absorption coefficient in an organic BHJ active layer is found for the intercalated blend system of PBTTT:PCBM [*Adv. Mater.* **2017**, *29*, 1702184.], which is only less than 5% of the singlet absorption coefficient of PBTTT. Therefore, for deriving the maximum value of E_{CT} of the solar cells studied in this work, we assume that the CT state EQE should contribute less than 10% of the single state EQE. This leads to a maximum value of E_{CT} of 1.41 eV for the solar cell based on PM7:Y5. Therefore, the range of the values for E_{CT} of the solar cell is restricted to 1.39 ± 0.02 eV.

E_{CT} of the solar cells based on PBDB-T:PM7:Y5 are also determined using the method described above. Results are shown below in Fig. S2.

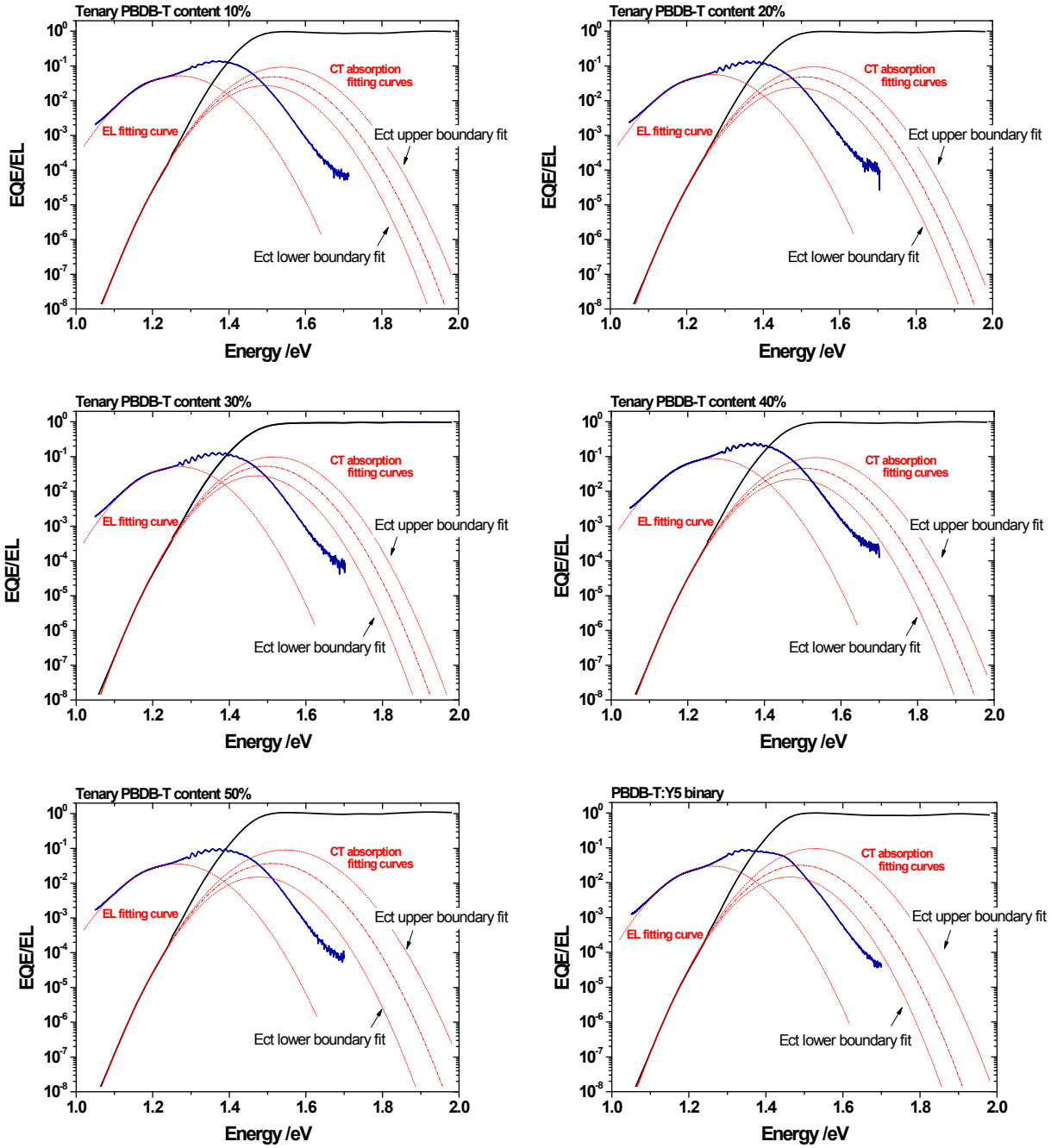

Fig. S2. EL and EQE spectra of the solar cells based on PBDB-T:PM7:Y5 with different PBDB-T contents.

SI-3. Optical bandgap of Y5 and absorption spectra of PM7 and PBDB-T

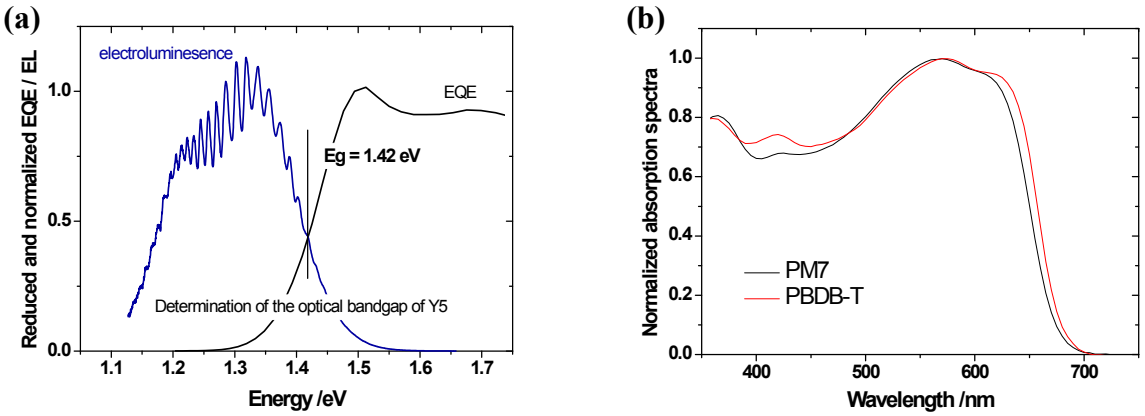

Fig. S3. a) The reduced and normalized EL and EQE spectra of a photovoltaic device based on pure Y5. The energy of the optical bandgap (E_g), defined as the transition energy between the lowest vibrational excited and ground states, is found at the crossing point between the reduced spectra. **b)** Absorption spectra of PM7 and PBDB-T.

SI-4. Internal quantum efficiency

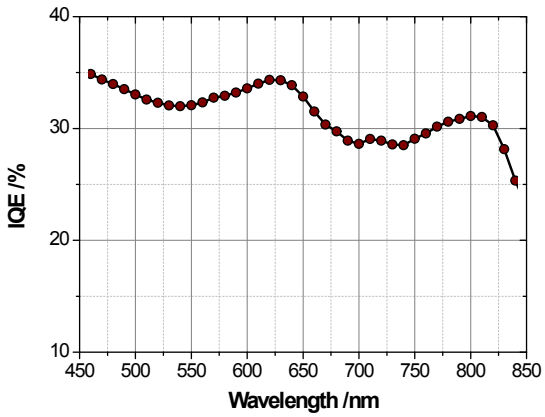

Fig. S4. Internal quantum efficiency of the organic solar cell based on PM7:Y5, calculated by dividing the measured EQE spectra by the EQE spectra simulated with a transfer matrix simulation. The optical constants of the active and passive materials in the solar cell stack are determined using spectroscopic ellipsometry.

SI-5. Atomic force microscopy

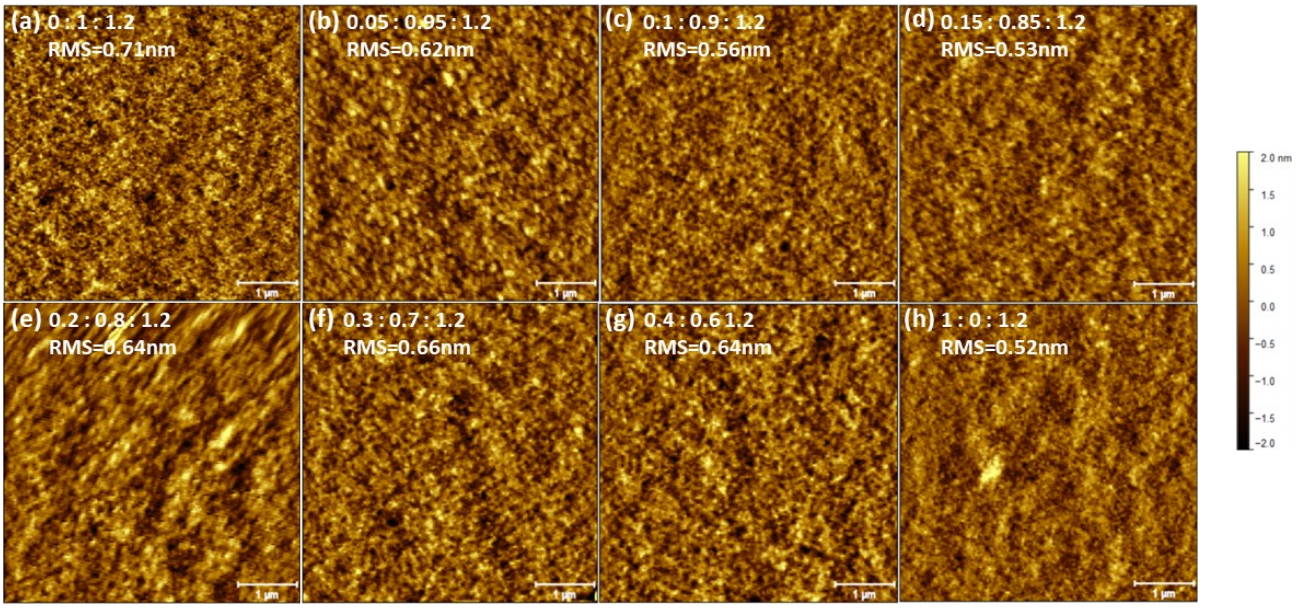

Fig. S5. AFM height images (size 5 µm x 5 µm) of the PBDB-T:PM7:Y5 based solar cells with different PBDB-T:PM7 donor ratios.

SI-6. Electric field dependent photoluminescence

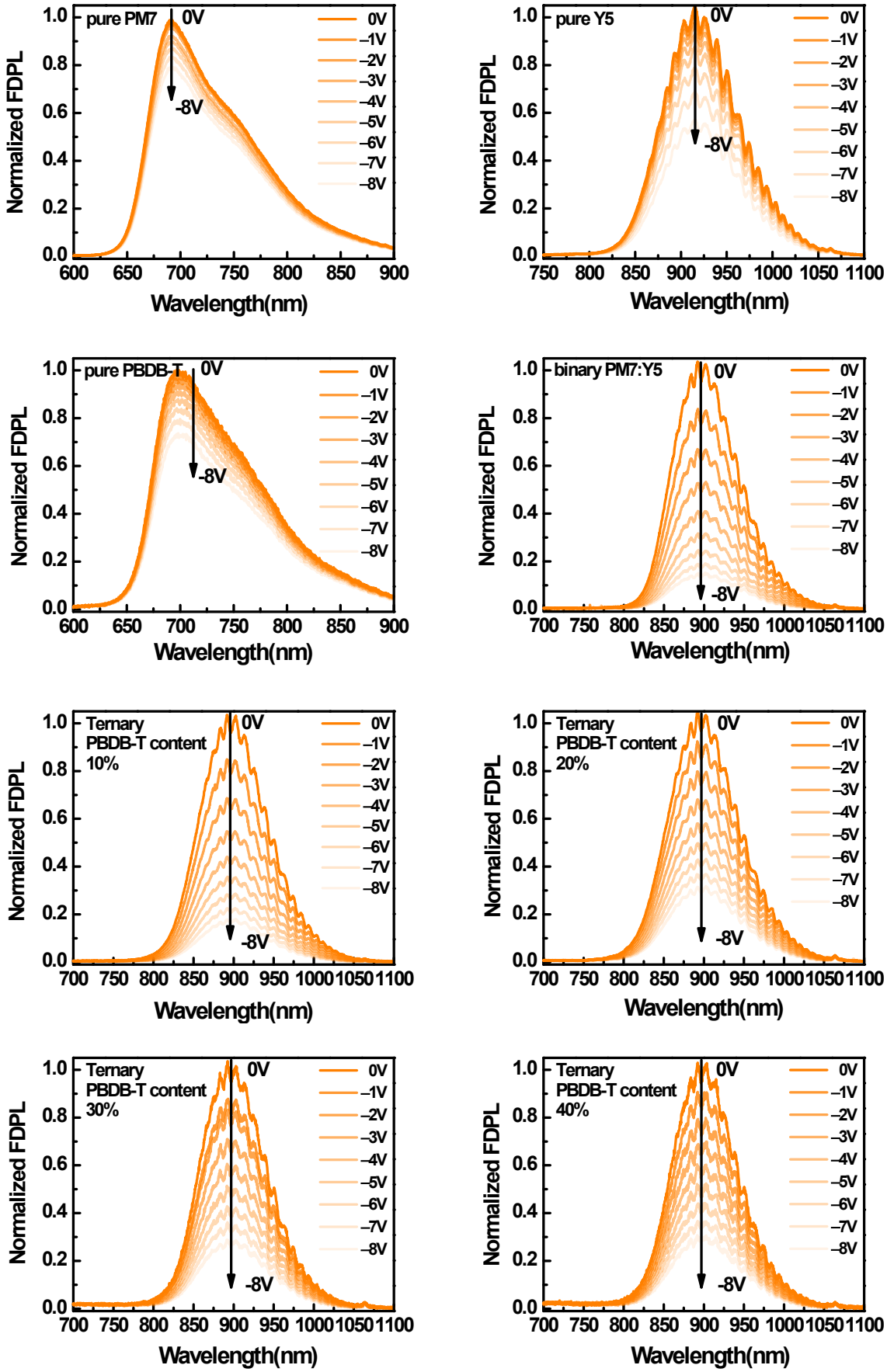

Fig. S6. PL spectra of the solar cells based on PBDB-T:PM7:Y5 with different PBDB-T contents, measured with different electric voltage bias.

SI-7. JV characteristic curves of organic solar cells

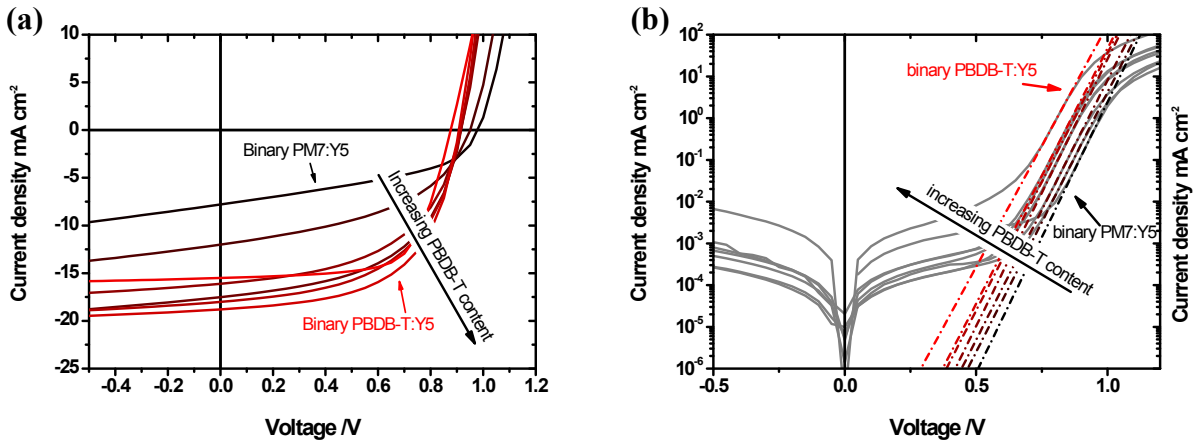

Fig. S7. JV characteristic curves of the solar cells based on PBDB-T:PM7:Y5 with different PBDB-T contents, measured **a)** under simulated AM1.5G illumination and **b)** in dark. The exponential regions of the dark JV curves are determined by the recombination current in the solar cells, and they can be fitted by a diode equation $J = J_0[\exp\left(\frac{qV}{nkT}\right) - 1]$, for the determination of the dark ideality factors (n) and dark saturation current (J_0) for the solar cells. The gradually shifting recombination current with the increasing PBDB-T content gives rise to increased J_0.

Table S7. Performance parameters of the ternary solar cells with different PBDB-T contents.

PBDB-T content	J_{sc} (mA cm^{-2})	V_{oc} (V)	FF (%)	PCE (%)	$E_{SI,A}$ (eV)	E_{CT} (eV)	ΔE_{CT} (eV)	V_{loss} (V)	$J_{0,rad}$ (mA cm^{-2})	$V_{oc,rad}$ (V)	$\Delta V_{nr}{}^{a}$ (V)	$\Delta V_{nr}{}^{b}$ (V)	EQE_{EL} (%)
0%	7.8	0.98	42.9	3.28	1.42	1.39	0.03	0.44	1.5x10^{-18}	1.10	0.12	0.13	0.751
10%	12.0	0.95	46.2	5.27	1.42	1.39	0.03	0.47	1.3x10^{-18}	1.10	0.15	0.16	0.142
20%	16.1	0.92	52.2	7.73	1.42	1.39	0.03	0.50	1.7x10^{-18}	1.09	0.17	0.18	0.062
30%	18.0	0.91	54.2	8.88	1.42	1.38	0.04	0.51	2.1x10^{-18}	1.09	0.17	0.19	0.044
40%	18.8	0.91	57.7	9.87	1.42	1.38	0.04	0.51	2.3x10^{-18}	1.09	0.19	0.20	0.036
50%	17.5	0.90	58.3	9.18	1.42	1.38	0.04	0.52	2.0x10^{-18}	1.09	0.20	0.21	0.024
100%	17.2	0.88	59.7	9.04	1.42	1.37	0.05	0.54	2.7x10^{-18}	1.08	0.21	0.22	0.015

a: ΔV_{nr} calculated from $J_{0,rad}$
b: ΔV_{nr} calculated from measured EQE_{EL}

SI-8. Electroluminescence external quantum efficiency measurements

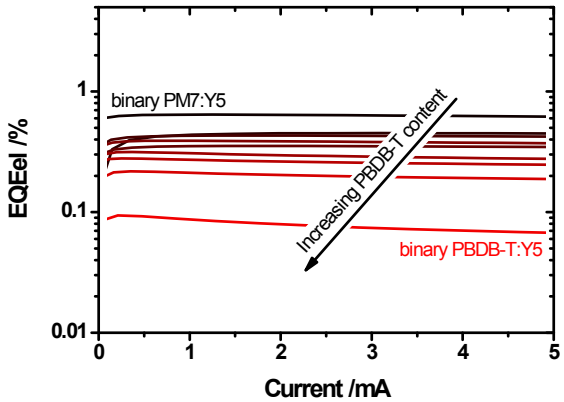

Fig. S8. EQE_{EL} of the solar cells based on PBDB-T:PM7:Y5 with different PBDB-T contents.

SI-9. Transient photovoltage decay measurements

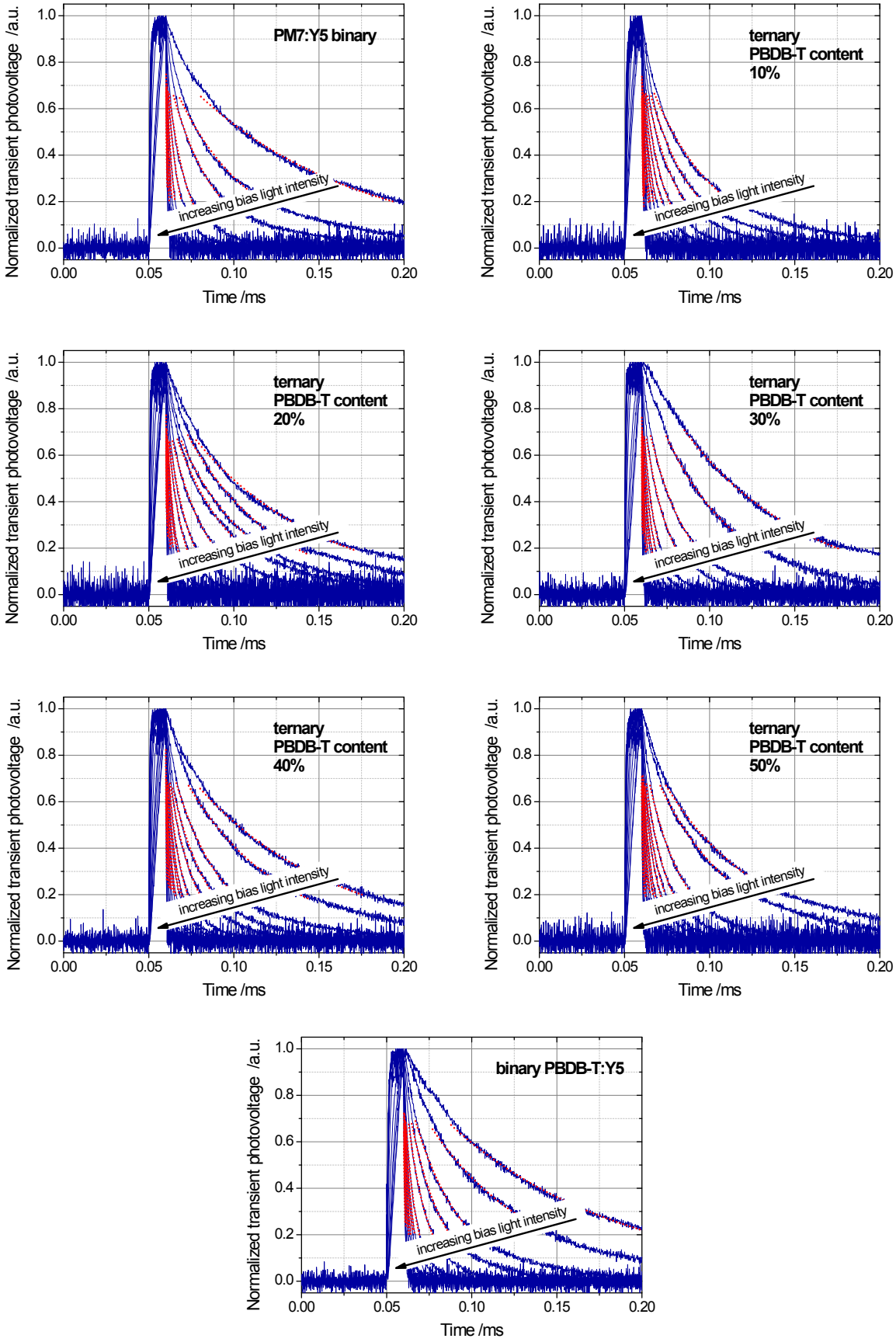

Fig. S9. Transient photovoltage decay of the solar cells based on PBDB-T:PM7:Y5 with different PBDB-T contents, measured with different bias illumination intensities. The decay time is obtained by an exponential fit.

SI-10. Energy levels of PBDB-T, PM7 and Y5

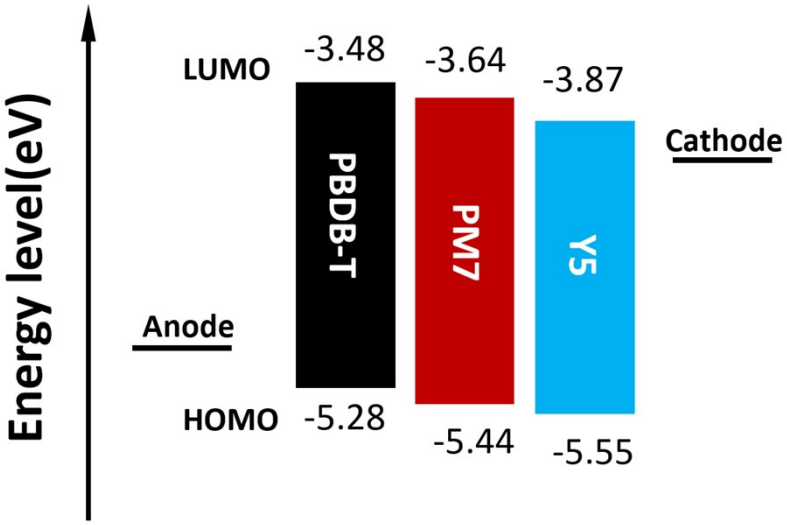

Fig. S10. Energy levels of the materials used in this work (J. Am. Chem. Soc. 2017, 139, 7148； Sci. China Chem. 2018, 61, 1328； Adv. Mater. 2019, 31, 1807577). The upper laying HOMO of PBDB-T (compared to that of PM7) gives rise to the lower E_{CT} in the binary blend of PBDB-T:Y5, allowing for the tuning of ΔE_{CT} of the ternary blend based on PM7:PBDB-T:Y5.

SI-11. Characterization of the devices based on pure PBDB-T, pure PM7 and the blend of PBDB-T:PM7

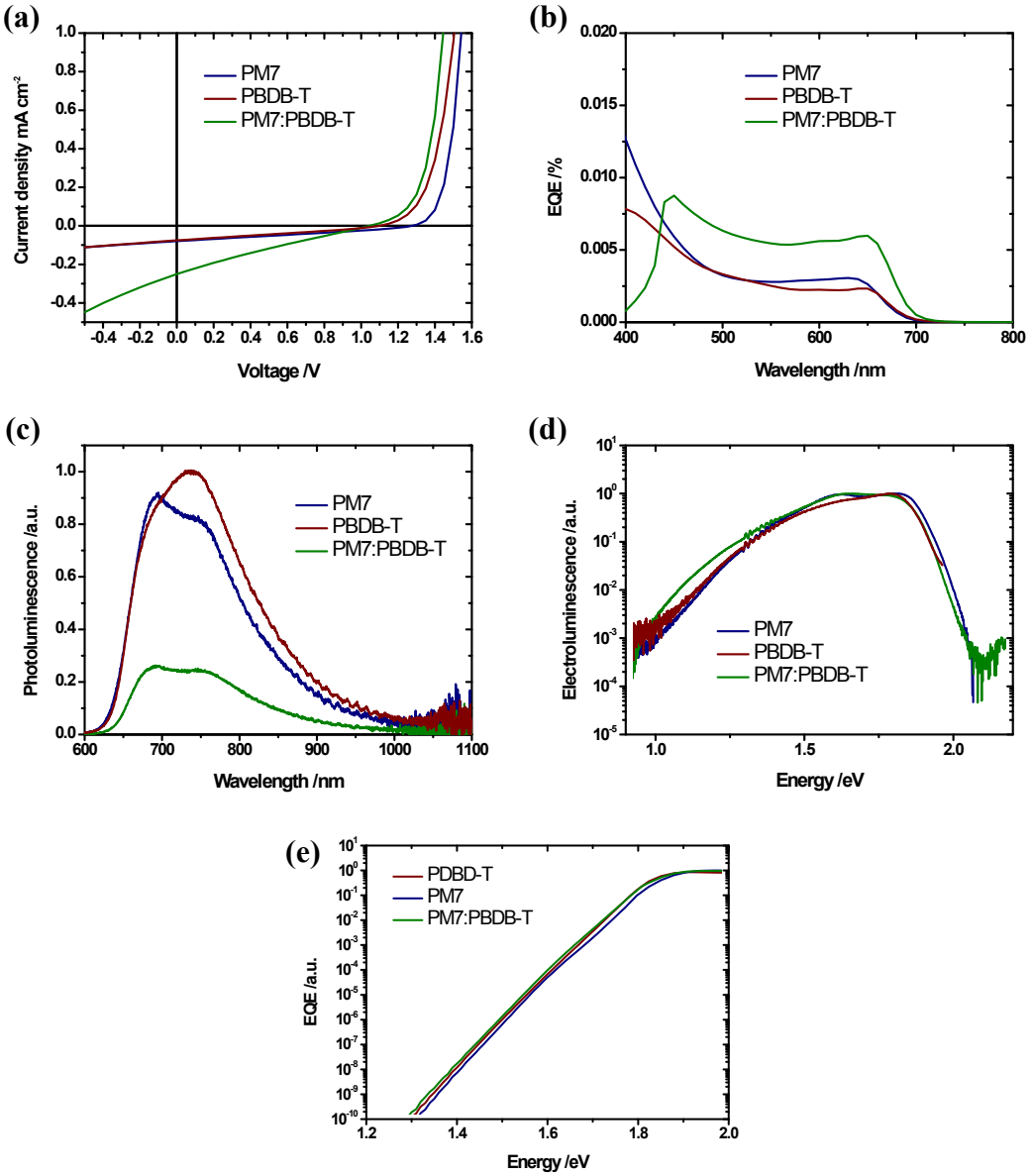

Figure S11. a) JV curves and **b)** EQE spectra of the devices based on PBDB-T, PM7, and the blend of PBDB-T:PM7 (1:1 weight ratio). **c)** Photoluminescence spectra of the thin films based on PBDB-T, PM7, and the blend of PBDB-T:PM7 (1:1), normalized to the emission peak of PM7, corrected by the absorbance of the films at the excitation wavelength (450 nm), **d)** Electroluminescence spectra (measured with an injection current of 1 mA) and **e)** Sensitive EQE spectra of the devices based on PBDB-T, PM7, and the blend of PBDB-T:PM7.